

## Atomic-scale dielectric permittivity profiles in slabs and multilayers

N. Shi and R. Ramprasad

*Department of Materials Science and Engineering, Institute of Materials Science, University of Connecticut, 97 North Eagleville Road, Storrs, Connecticut 06269, USA*

(Received 17 February 2006; revised manuscript received 27 April 2006; published 19 July 2006)

A recently developed theory of atomic-scale local dielectric permittivity has been used to determine the position dependent permittivity profiles of a few nanoscale insulator surfaces and multilayers. Specifically, slabs containing single-component (Si, polymer, and SiO<sub>2</sub>) and two-component (Si-SiO<sub>2</sub> and polymer-SiO<sub>2</sub>) systems of technological importance have been studied. The present approach indicates that the local permittivity is generally enhanced at the surfaces and/or interfaces, and that it approaches the corresponding bulk values in the interior of each component. This simple method of determining the position-dependent dielectric permittivity profiles can be used to study the impact of atomic level disorder and defects on dielectric properties.

DOI: [10.1103/PhysRevB.74.045318](https://doi.org/10.1103/PhysRevB.74.045318)

PACS number(s): 78.20.Bh, 77.55.+f, 77.84.Jd

### I. INTRODUCTION

Thin films based on high dielectric constant (high- $k$ ) materials have attracted great attention in recent years as they could potentially allow continued lateral size shrinkages of microelectronics devices such as transistors, capacitors, etc.<sup>1,2</sup> Also, nanocomposites based on polymers and high- $k$  oxide dielectrics are being considered for the creation of flexible organic substrates as the dielectric constant of the substrate can potentially be increased without compromising its flexibility.<sup>3-8</sup> In both these examples, surface and interface effects are expected to play a dominant role in determining the dielectric properties, especially as the system sizes (i.e., the thickness of the dielectric films in multilayer stacks, or the size of dielectric oxide particles in nanocomposites) approach the nanoscale regime. Thus, while in the macroscopic regime, the average permittivity of multicomponent systems can be determined from the permittivity of the respective bulk materials, such an approach will be inadequate at nanometer length scales.

In fact, observations suggest that the permittivity of ultrathin SiO<sub>2</sub> deposited on Si is appreciably higher at the Si-SiO<sub>2</sub> interface than that of bulk SiO<sub>2</sub>.<sup>9,10</sup> This observation has also been confirmed by first principles calculations of the local dielectric permittivity.<sup>11,12</sup> Furthermore, it has been recently observed that the effective permittivity of polymer-oxide composites can be significantly higher than that expected given the permittivity of the corresponding single component bulk values.<sup>6</sup> This increase in effective permittivity has also been correlated with the total surface area of the interface (which increases as the oxide particle sizes decrease). An understanding of the dielectric properties of these systems calls for an accurate determination of atomic-scale dielectric permittivity profiles across layered structures.

In principle, the dielectric response is completely accounted for by the nonlocal dielectric tensor. However, the calculation of this quantity for complex systems is computationally demanding, and often carries excessively detailed information with respect to experimental interests. Recently, Giustino *et al.*<sup>11,12</sup> have introduced a practical method for the calculation of the position dependent dielectric permittivity

of multilayer systems in the presence of finite electric fields. Two approaches to determining the local permittivity were introduced in this prior work:<sup>12</sup> one based on the berry phase technique applicable to periodic multilayer stacks, and a second one applicable to systems in slab geometries with intervening vacuum regions. The former was used to study a Si-SiO<sub>2</sub> interface, and the latter to study Si slabs. Both techniques go beyond the traditional ways of determining the dielectric permittivity of bulk<sup>13-21</sup> and superlattice<sup>22</sup> systems and more recent ways of indirectly determining the surface or interface contributions to the total field-induced polarizations by considering films of varying thickness.<sup>23,24</sup> It is also worth mentioning that techniques closely related to the latter method of Giustino and Pasquarello<sup>12</sup> were used in the determination of the local dielectric response of Si<sup>25</sup> and GaAs<sup>26</sup> nanostructures.

The simplicity of this latter method to determine the local position dependent permittivity arises from the fact that most standard DFT implementations can be used as-is without the need for additional major code development; more importantly, this approach can treat finite systems such as slabs, with the bulk dielectric properties (optical and static) resulting as a by-product. A local permittivity function was introduced to describe variations of the dielectric response over length scales of the order of interatomic distances, which can conveniently be calculated from the local field induced self-consistent charge density profile. The optical part of the position dependent polarization and permittivity is obtained in terms of the field-induced displacements of just the electronic charge density (with the ions held fixed at their field-free equilibrium positions), while the static part is determined from both the induced electronic and ionic displacements.

The primary goal of the present work is to use the latter scheme proposed by Giustino and Pasquarello<sup>12</sup> to determine the position dependent dielectric permittivity profiles of a variety of single and two-component systems of technological importance. First we consider three different slab systems with finite thickness: Si, SiO<sub>2</sub>, and polymer. In general, we find that the local permittivity in the slab interior approaches the corresponding bulk values within a few atomic layers from the surfaces. Second, two different interfaces are con-

sidered: Si-SiO<sub>2</sub> and SiO<sub>2</sub>-polymer. We show that bulk permittivities are recovered within distances from the interface corresponding to a few bond lengths and that the local permittivity is enhanced in the interfacial suboxide region.

The present paper is organized as follows. Section II outlines the theory, as implemented here, for obtaining the local permittivity profile, closely following the prior development.<sup>12</sup> In Sec. III, we specify the technical details of our computational approach. Section IV is devoted to applications to Si, SiO<sub>2</sub>, and polymer slabs, as well as to the Si-SiO<sub>2</sub> and SiO<sub>2</sub>-polymer interfaces. Finally, our conclusions are drawn in Sec. V.

## II. THEORY OF LOCAL PERMITTIVITY

From the in-medium Maxwell equation, the induced microscopic polarization  $\mathbf{p}(\mathbf{r})$  can be obtained from the induced charge density  $\rho_{ind}(\mathbf{r})$  through the Gauss relation<sup>28</sup>

$$\nabla \cdot \mathbf{p}(\mathbf{r}) = -\rho_{ind}(\mathbf{r}). \quad (1)$$

In this work, we are primarily interested in multilayer geometries periodic along the  $x$ - $y$  plane, with the surface or interface normal aligned along the  $z$  direction. For such a quasi-one-dimensional system, Eq. (1) reduces to

$$\frac{d}{dz}\bar{p}(z) = -\bar{\rho}_{ind}(z), \quad (2)$$

where the  $\bar{p}(z)$  and  $\bar{\rho}_{ind}(z)$  are the polarization and induced charge density, respectively, averaged along the  $x$ - $y$  plane. The induced charge density  $\bar{\rho}_{ind}(z)$  can be evaluated by applying finite electric fields of  $\pm\delta$  along the  $z$  direction and taking the differences of the resulting charge densities for the positive and negative fields. The solution of Eq. (2) is the following:

$$\bar{p}(z) = \bar{p}_{-\infty} - \int_{-\infty}^z \bar{\rho}_{ind}(z') dz'. \quad (3)$$

Assuming that our slab of finite thickness is placed at  $z > 0$ , the constant  $\bar{p}_{-\infty}$  can be set to zero as it corresponds to the polarization at  $-\infty$ , a region where charge density is zero.

Using the above procedure, both the optical (high frequency) and the static (low frequency) microscopic polarization can be calculated. For the optical case, the atoms are fixed at their field-free equilibrium positions, and only the electronic degrees of freedom are allowed to relax in response to the applied electric field, as in the high frequency limit, we expect only the electrons to respond to the external electric field. For the static case, both the electrons and ions are allowed to respond to the electric field. Finally, in supercell slab calculations where the polarization is induced due to both the external electric field and the periodic image dipoles, the true polarization due to just the external electric field can be obtained using a simple scaling procedure described earlier.<sup>23,24</sup>

The calculated polarization profile can then be used to determine the position dependent local (relative) permittivity (or dielectric constant), using

$$\epsilon(z) = \frac{\partial \bar{p}(z)}{\epsilon_0 \partial E_{loc}(z)} + 1, \quad (4)$$

where  $\epsilon_0$  is the permittivity of free, and  $E_{loc}(z)$  is the local electric field given by  $E_{loc}(z) = E_{ext} - \bar{p}(z)/\epsilon_0$ , with  $E_{ext}$  being the external electric field. For linear dielectrics, such as the ones considered here,  $\partial \bar{p}(z)/\partial E_{loc}(z) = \bar{p}(z)/E_{loc}(z)$ , and Eq. (4) reduces to

$$\epsilon(z) = \frac{\epsilon_0 E_{ext}}{\epsilon_0 E_{ext} - \bar{p}(z)}. \quad (5)$$

In the present work,  $E_{ext} = 2\delta$ , as  $\bar{p}(z)$  was determined from charge densities due to fields of  $+\delta$  and  $-\delta$  along the  $z$  direction separately. Using  $\bar{p}(z)$  corresponding to the optical and static cases results, respectively, in the optical and static local permittivities.

## III. METHOD AND MODELS

All calculations presented here were performed using the local density approximation (LDA) within DFT (Ref. 27) as implemented in the local orbital SIESTA code.<sup>29</sup> Norm-conserving nonlocal pseudopotentials of the Troullier-Martins type were used to describe all the elements. The atomic configuration [Ne]3s<sup>2</sup>3p<sup>2</sup> was used for the Si pseudopotential, [He]2s<sup>2</sup>2p<sup>4</sup> for the O pseudopotential, [He]2s<sup>4</sup> for the C pseudopotential, and [H] for H pseudopotential. Semi-core corrections were used for Si. A double-zeta plus polarization (DZP) basis set with orbital-confining cutoff radii was determined by a PAO. Energyshift parameter of 0.0001 Ry was used for all calculations. SiO<sub>2</sub> in the  $\alpha$ -quartz and  $\beta$ -cristobalite phases were considered. 75 and 64 special  $\mathbf{k}$  points, respectively, yielded well converged bulk and slab results for Si. The corresponding number of special  $\mathbf{k}$  points that resulted in converged results for SiO<sub>2</sub> in the  $\beta$ -cristobalite phase were 108 and 36, and those for SiO<sub>2</sub> in the  $\alpha$ -quartz phase were 74 and 23. 18 special  $\mathbf{k}$  points yielded well converged polymer slab results. The equilibrium positions of all the atoms were determined by requiring the forces on each atom to be smaller than 0.01 eV/Å.

The equilibrium lattice constant of Si in the diamond crystal structure was calculated here to be 5.43 Å, which agrees well with prior DFT calculations (5.48 Å) (Refs. 11, 12, and 30) and experiments (5.43 Å).<sup>31,32</sup> The equilibrium lattice constants,  $a$  and  $c$ , in  $\alpha$ -quartz SiO<sub>2</sub> calculated here to be 4.91 Å and 5.41 Å, respectively, also agree well with prior DFT calculations (5.02 Å and 5.53 Å),<sup>33,34</sup> and with experimental results (4.92 Å and 5.41 Å).<sup>35</sup> For  $\beta$ -cristobalite, the calculated lattice constant was 7.49 Å, in reasonable agreement with other theory (7.14 Å),<sup>36</sup> and experiments (7.17 Å).<sup>37</sup> A C<sub>12</sub>H<sub>26</sub> hydrocarbon chain was used to model a polymer. The calculated C-C and C-H bond distances were 1.52 Å and 1.12 Å, in good agreement with the experiments (1.54 Å and 1.10 Å).<sup>38</sup> For all slab calculations, the equilibrium atomic positions in the absence of an external electric field (including surface relaxation and reconstructions), was first determined. Electric field of strength  $\pm 0.01$  eV/Å was then applied, and the resulting total charge

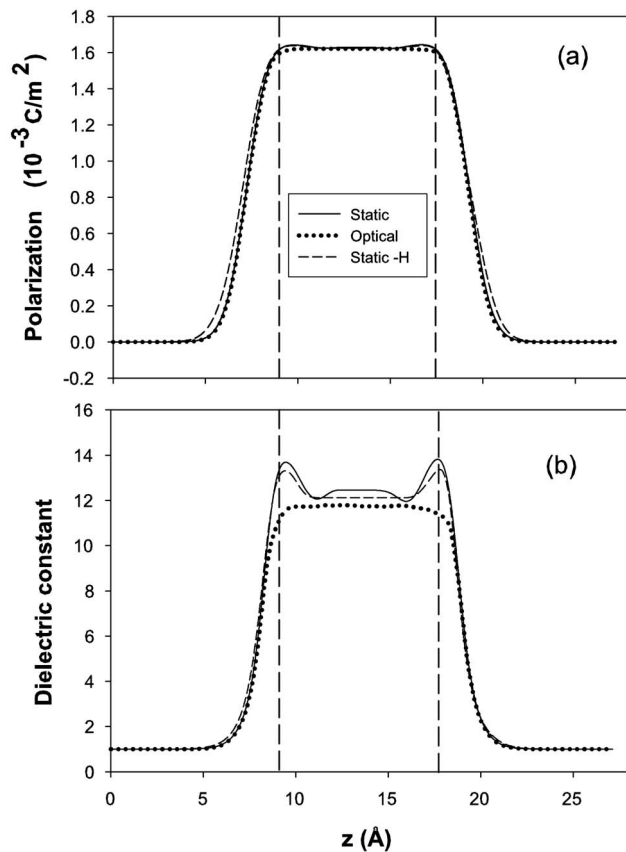


FIG. 1. Static (solid) and optical (dotted) planar-averaged polarization (a) and dielectric constant (b) of a Si (001) slab as a function of position  $z$  normal to the slab surface. The static polarization and dielectric constant when the surface Si atoms are passivated by H atoms are also shown (dashed lines).

density was used to calculate the optical and static local polarizations and permittivity.

#### IV. RESULTS

Below we present the results for the Si,  $\text{C}_{12}\text{H}_{26}$ ,  $\beta$ -cristobalite, and  $\alpha$ -quartz 1-component slabs first, before describing interfaces created from these slabs.

##### A. Si and $\text{C}_{12}\text{H}_{26}$ (polymer) slabs

A Si(001) slab with a finite thickness of 10.96 Å containing nine layers of Si along the  $z$  direction, and a  $2 \times 2$  unit cell along the surface plane was considered. The slab was terminated on both sides by Si atoms, and the atomic coordinates were first optimized in the absence of an external electric field. Following the procedure outlined in Sec. II, the planar-averaged induced charge density and the local polarization were calculated due to the application of an external field of strength  $\pm 0.01 \text{ eV/\AA}$ ; the calculated polarization profiles were then used to determine the permittivity profiles using Eq. (5). The calculated planar averaged polarization  $[\bar{p}(z)]$  and dielectric constant  $[\epsilon(z)]$  profiles along the  $z$  direction are shown in Fig. 1; the legends “optical” and “static” refer, respectively, to the cases when the atoms were fixed at

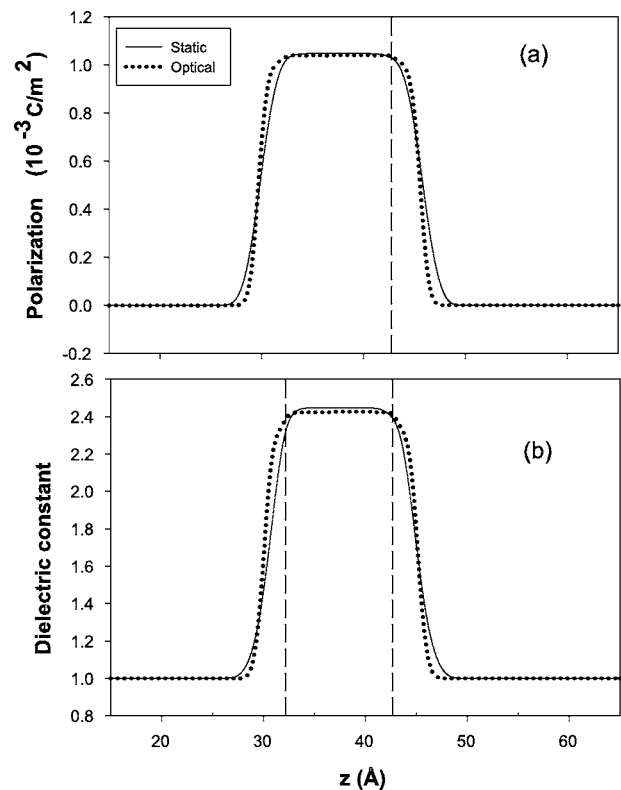


FIG. 2. Static (solid) and optical (dotted) planar-averaged polarization (a) and dielectric constant (b) of a periodic arrangement of hydrocarbon chains as a function of position  $z$  along the chain axis.

their field-free equilibrium positions, and when they were allowed to relax to their field-induced equilibrium positions. The legend “static-H” refers to the case when all the silicon atoms in the surface planes were passivated with H atoms. From the figure, we can see that the dielectric constant in the inner layers away from the surface approach the bulk Si value of about 12 for both optical and static cases, in good agreement with experimental estimates.<sup>39</sup> At the region within 3 Å of the surfaces, the polarization and dielectric constant increase from the bulk values in the static case due to the emergence of ionic character of bonds close to the surface. Termination of the free slab surfaces with H atoms results in a small reduction in the polarization and dielectric constant enhancement at the slab surfaces. The calculated polarization and dielectric constant profiles are in good agreement with the results of Giustino and Pasquarello,<sup>12</sup> calculated using a similar method as here, as well as with the results of Delerue *et al.*<sup>25</sup>

A  $\text{C}_{12}\text{H}_{26}$  molecule arranged in a square lattice with dimensions  $4.91 \text{ \AA} \times 4.91 \text{ \AA} \times 81.2 \text{ \AA}$  and its chain axis along the  $z$  direction was used as a model of a bulk polymer. Figure 2 shows the calculated planar averaged polarization and dielectric constant profiles along the  $z$  direction. From the figure, we can see that the dielectric constant in the interior of the chains approaches a constant value of about 2.4 for both optical and static properties. Although it is not clear whether the volume fraction (or density) of the polymers modeled here is meaningful from an experimental standpoint, we mention that the experimental estimates of the dielectric con-

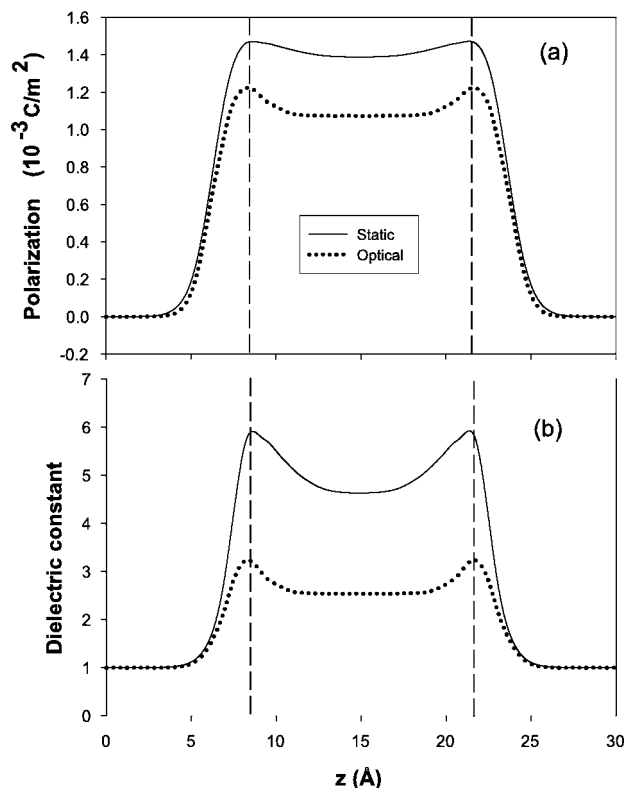


FIG. 3. Static (solid) and optical (dotted) planar-averaged polarization (a) and dielectric constant (b) of a (001)  $\beta$ -cristobalite  $\text{SiO}_2$  slab as a function of position  $z$  normal to the interface.

stant of hydrocarbon based polymeric materials is in the 2.0–2.2 range.<sup>40</sup> We also observe that the polarization and dielectric constant profiles drop off smoothly to the vacuum values from their “bulk” values, in contrast to the behavior of the Si slabs discussed above, presumably due to the fact that *all* the C atoms (including the ones at the ends of the chain) are in a similar tetrahedral coordination environment.

### B. $\text{SiO}_2$ slabs: $\beta$ -cristobalite and $\alpha$ -quartz

Si-terminated (001)  $\beta$ -cristobalite and (0001)  $\alpha$ -quartz slabs were considered next, with thickness along the  $z$  direction of 14.98 and 16.24 Å, respectively. These thicknesses were found to be sufficient to ensure a bulklike region in the interior of the slabs, as evidenced by negligible surface relaxations in the interior, under field-free conditions.<sup>24</sup> The calculated field-induced local planar averaged polarization and dielectric constant profiles for the  $\beta$ -cristobalite and  $\alpha$ -quartz slabs are shown in Figs. 3 and 4, respectively. As with silicon slabs, we see that the polarization and dielectric constant attain constant values in the interior of the slabs, with an enhancement of these quantities in the surface regions. The optical and static dielectric constants for  $\beta$ -cristobalite, extracted from the interior of slabs were 2.5 and 4.5, respectively, and those for  $\alpha$ -quartz were 2.6 and 4.6, respectively, all in good agreement with experimental determinations.<sup>41,42</sup>

### C. Si- $\text{SiO}_2$ interface

The results given in the previous sections provide us with some of the ingredients needed for predicting the dielectric

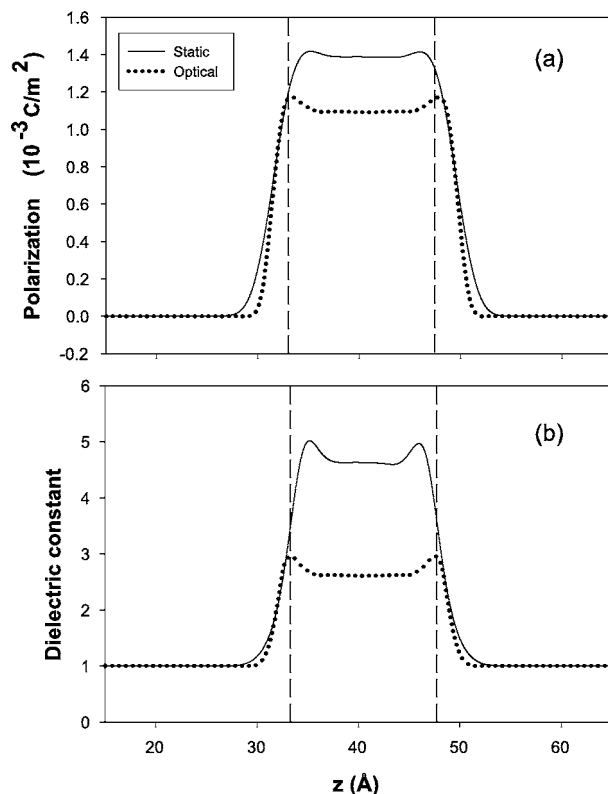


FIG. 4. Static (solid) and optical (dotted) planar-averaged polarization (a) and dielectric constant (b) of a (0001)  $\alpha$ -quartz  $\text{SiO}_2$  slab as a function of position  $z$  normal to the interface. (b) Static (solid) and optical (dotted) dielectric constant as a function of position  $z$  along normal to the interface.

properties of the Si- $\text{SiO}_2$  multilayers. The Si- $\text{SiO}_2$  interface has been studied for many decades due to their use in metal-oxide-semiconductor field effect transistors. Here we consider a Si- $\text{SiO}_2$  interface composed of crystalline Si and  $\text{SiO}_2$ , of thickness 10.96 and 14.70 Å, respectively, with the latter in the  $\beta$ -cristobalite phase. The Si lattice parameter was fixed at 5.43 Å, corresponding to our predicted equilibrium value. The (001) face of  $\beta$ -cristobalite was lattice matched and placed along the diagonal of the (001)-surface unit cell of the Si slab. Thus, we constrain the lattice constant of  $\text{SiO}_2$  to  $\sqrt{2}$  times the lattice constant of Si, i.e., 7.68 Å, which is only about 2.5% larger than the equilibrium lattice constant of  $\beta$ -cristobalite as determined here. For this choice of constrained lattice constant along the (001) plane, the lattice parameter of the oxide in the [001] direction determined by a separate calculation was 7.35 Å, with a Si-O bond length of 1.63 Å, Si-O-Si angles of 178.4°, and O-Si-O angles of 114.7° and 109.3°, close to the corresponding equilibrium bulk values.

In order to obtain a structural transition without coordination defects between the silicon and its oxide in our model interface, we adopt a bridging oxygen model (BOM) for the interface described earlier.<sup>36</sup> The thickness of the suboxide region within this model is about 3 Å, and all the partial oxidation states of Si (namely, Si,  $\text{Si}^+$ ,  $\text{Si}^{2+}$ , and  $\text{Si}^{3+}$ ) appear in equal amounts in the suboxide region.

Figure 5 shows the polarization and dielectric constant profiles as a function of position along the direction normal

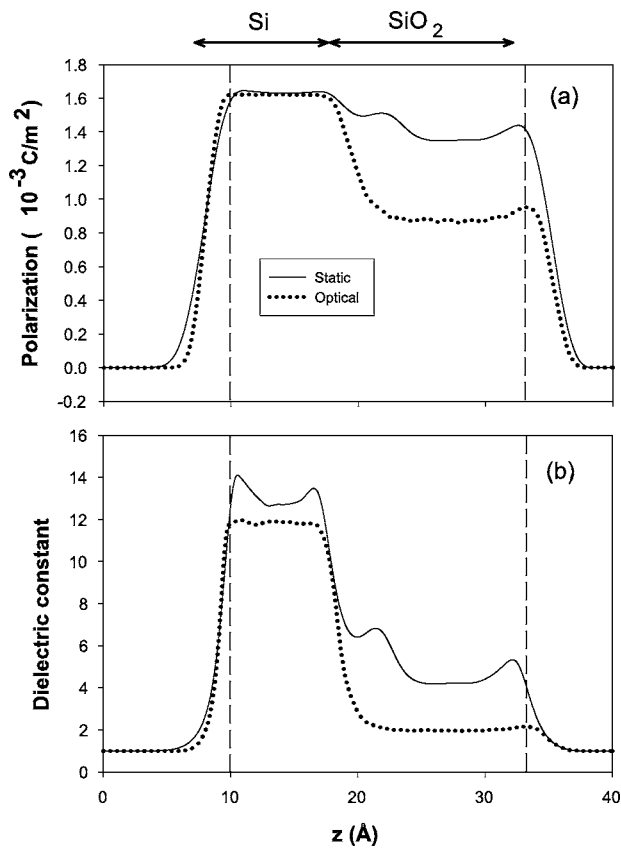


FIG. 5. Static (solid) and optical (dotted) planar-averaged polarization (a) and dielectric constant (b) for the Si-SiO<sub>2</sub> stack as a function of position along a direction normal to the interface. SiO<sub>2</sub> is in the  $\beta$ -cristoballite phase.

to Si-SiO<sub>2</sub> interface. This same interface has been studied earlier, and polarization and dielectric constant profiles have been determined using the berry phase method.<sup>11,12</sup> As shown in Fig. 5, for the combined two-component system, the dielectric properties in the interior of the SiO<sub>2</sub> and Si regions match perfectly with the properties of SiO<sub>2</sub> and Si taken separately. However, in the transition region between Si and SiO<sub>2</sub> that contains the entire interfacial oxide, we find that there is an enhancement of the static polarization and the dielectric constant, compared to those of the bulk and the oxide free surface. The deviation at the interface is due to the Si atoms that exist in partial oxidation states as pointed out earlier,<sup>11,12</sup> and is also consistent with prior experimental<sup>9</sup> results.

#### D. Polymer-SiO<sub>2</sub> ( $\alpha$ -quartz) interface

We then studied the two-component polymer-SiO<sub>2</sub> chain system. Here, SiO<sub>2</sub> was assumed to be in the  $\alpha$ -quartz phase, and the polymer chain was approximated by a -C<sub>12</sub>H<sub>25</sub> molecule with a dangling bond. The end C atom of the -C<sub>12</sub>H<sub>25</sub> chain with a dangling bond was bonded to a surface Si atom of  $\alpha$ -quartz, and the structure was optimized in the absence of an external electric field. The relaxed interface was characterized by an O-Si-C angle of 113.0°, and a C-Si bond length of 1.89 Å. The first C-C bond length away from

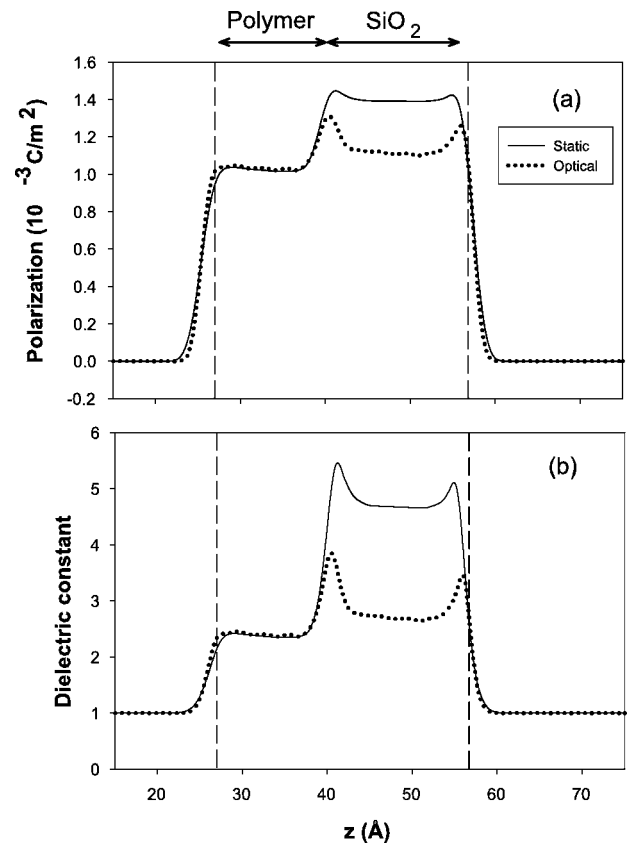


FIG. 6. Static (solid) and optical (dotted) planar-averaged polarization (a) and dielectric constant (b) for the C<sub>12</sub>H<sub>25</sub>-SiO<sub>2</sub> stack as a function of position along a direction normal to the interface. SiO<sub>2</sub> is in the  $\alpha$ -quartz phase.

the interface within the hydrocarbon chain was 1.52 Å, the C-C-C angle along the axis was 112.0°, and the C-H bond length was 1.12 Å, characteristic of the isolated hydrocarbon chain.

Figure 6 shows the local polarization and dielectric constant as a function of position along the slab surface normal for the polymer-SiO<sub>2</sub> system. We observe similar behavior of the dielectric constants as with the Si-SiO<sub>2</sub> interface. The dielectric constant in the interior of the SiO<sub>2</sub> and polymer chain regions match well with the corresponding experimental single component bulk values and there is an enhancement of the dielectric constant, compared to the one-component results at the interfaces and surface. In contrast to the Si-SiO<sub>2</sub> interface, the enhancement in the dielectric constant at the polymer-SiO<sub>2</sub> interface is almost entirely in the SiO<sub>2</sub> side of the interface. Analysis of the Mulliken charges of the atoms indicates that the C atoms closest to the interface are in their nominal oxidation states (i.e., in oxidation states similar to that of C atoms in the interior of the polymer chain), whereas the Si and O atoms close to the interface are in varying oxidation states similar to that in the Si-SiO<sub>2</sub> case<sup>12</sup> (see also Sec. IV C). This is consistent with the deviation of the dielectric constant from the corresponding bulk value only on the SiO<sub>2</sub> side of the interface. It is likely that such a behavior is specific to the polymer-oxide interface model chosen here. Nevertheless, an enhancement of the di-

electric constant at the SiO<sub>2</sub> side of the interface is expected to occur in general, as the Si-O bond is more polar than the bonds in polymer chains. Although a quantitative comparison with experiments concerning the enhancement in dielectric constants cannot be performed due to the unavailability of specific experimental data, it is worth mentioning that the calculated enhancement at the interface is consistent with recent experimental work on polymer-oxide composites, which display effective permittivities noticeably higher than that expected given the permittivity of the corresponding single component bulk values.<sup>6</sup>

While we have demonstrated the applicability of this method for just a few restricted situations, we believe that this simple procedure for calculating the position-dependent dielectric properties has a broader appeal. It can be systematically used in a study of the impact of a wide variety of interfaces and other types of atomic level disorder on the dielectric properties.

### V. SUMMARY

In summary, we have used standard density functional theory based calculations to study the dielectric properties of

nanoscale multilayer multicomponent systems. We have calculated the local polarization and dielectric constant profiles over length scales of the order of interatomic distances for several one-component slab (Si, polymer, and SiO<sub>2</sub>) and two two-component slab (Si-SiO<sub>2</sub> and polymer-SiO<sub>2</sub>) systems, using the charge density induced by an external constant finite electric field. We find that the local polarization and permittivity values approach that of the corresponding bulk systems within a few bulk interatomic spacings of the surfaces and/or interfaces. The calculated bulk optical and static electronic dielectric constant values are in excellent agreement with the experimental results and other more involved computational treatments. This work forms the groundwork for a more thorough analysis of the impact of surfaces, interfaces, and atomic level defects on the dielectric properties of a wide variety of nanostructured systems.

### ACKNOWLEDGMENTS

Partial support of this work by grants from the ACS Petroleum Research Fund and the Office of Naval Research is gratefully acknowledged.

- 
- <sup>1</sup>G. D. Wilk, R. M. Wallace, and J. M. Anthony, *J. Appl. Phys.* **89**, 5243 (2001).  
<sup>2</sup>A. I. Kingon, J. P. Maria, and S. K. Streiffer, *Nature (London)* **406**, 1032 (2000).  
<sup>3</sup>S. S. Ray and M. Okamoto, *Prog. Polym. Sci.* **28**, 1539 (2003).  
<sup>4</sup>Y. Rao and C. P. Wong, *J. Appl. Polym. Sci.* **92**, 2228 (2004).  
<sup>5</sup>S. O'Brien, L. Brus, and C. B. Murray, *J. Am. Chem. Soc.* **123**, 12085 (2001).  
<sup>6</sup>P. Murugaraj, D. Mainwaring, and N. Mora-Huertas, *J. Appl. Phys.* **054304**, 98 (2005).  
<sup>7</sup>Y. Vo and C. P. Wong, *J. Appl. Polym. Sci.* **2228**, 92 (2004).  
<sup>8</sup>R. C. Advincula, *J. Dispersion Sci. Technol.* **24**, 343 (2003).  
<sup>9</sup>C. M. Perkins, B. B. Triplett, P. C. McIntyre, K. C. Saraswat, S. Haukka, and M. Touminen, *Appl. Phys. Lett.* **78**, 2357 (2001).  
<sup>10</sup>H. S. Chang, H. D. Yang, H. Hwang, H. M. Cho, H. J. Lee, and D. W. Moon, *J. Vac. Sci. Technol. B* **20**, 1836 (2002).  
<sup>11</sup>F. Giustino, P. Umari, and A. Pasquarello, *Phys. Rev. Lett.* **91**, 267601 (2003).  
<sup>12</sup>F. Giustino and A. Pasquarello, *Phys. Rev. B* **71**, 144104 (2005).  
<sup>13</sup>F. Detraux, Ph. Ghosez, and X. Gonze, *Phys. Rev. Lett.* **81**, 3297 (1998).  
<sup>14</sup>R. H. French, S. J. Glass, F. S. Ohuchi, Y. N. Xu, and W. Y. Ching, *Phys. Rev. B* **49**, 5133 (1994).  
<sup>15</sup>G.-M. Rignanese, F. Detraux, X. Gonze, and A. Pasquarello, *Phys. Rev. B* **64**, 134301 (2001).  
<sup>16</sup>P. Umari and A. Pasquarello, *Phys. Rev. Lett.* **89**, 157602 (2002).  
<sup>17</sup>H. Fu and L. Bellaiche, *Phys. Rev. Lett.* **91**, 057601 (2003).  
<sup>18</sup>K. Kunc and R. Resta, *Phys. Rev. Lett.* **51**, 686 (1983).  
<sup>19</sup>R. D. King-Smith and D. Vanderbilt, *Phys. Rev. B* **47**, 1651 (1993).  
<sup>20</sup>X. Zhao and D. Vanderbilt, *Phys. Rev. B* **65**, 233106 (2002).  
<sup>21</sup>X. Zhao and D. Vanderbilt, *Phys. Rev. B* **65**, 075105 (2002).  
<sup>22</sup>Silvana Botti, Nathalie Vast, Lucia Reining, Valerio Olevano, and Lucio Claudio Andreani, *Phys. Rev. Lett.* **89**, 216803 (2002).  
<sup>23</sup>R. Ramprasad and N. Shi, *Phys. Rev. B* **72**, 052107 (2005).  
<sup>24</sup>N. Shi and R. Ramprasad, *Appl. Phys. Lett.* **87**, 262102 (2005).  
<sup>25</sup>C. Delerue, M. Lannoo, and G. Allan, *Phys. Rev. B* **68**, 115411 (2003).  
<sup>26</sup>Xavier Cartoixa and Lin-Wang Wang, *Phys. Rev. Lett.* **94**, 236804 (2004).  
<sup>27</sup>R. Martin, *Electronic Structure: Basic Theory and Practical Methods* (Cambridge University Press, New York, 2004).  
<sup>28</sup>J. D. Jackson, *Classical Electrodynamics* (University of California, Berkeley, 1998).  
<sup>29</sup>J. M. Soler, E. Artacho, J. Gale, A. Garcia, J. Junquera, P. Ordejon, and D. Sanchez-Portal, *J. Phys.: Condens. Matter* **14**, 2745 (2002).  
<sup>30</sup>T. A. Kirichenko, D. Yu, S. K. Banerjee, and G. S. Hwang, *Phys. Rev. B* **72**, 035345 (2005).  
<sup>31</sup>J. Wang, H. Li, and R. Stevens, *J. Mater. Sci.* **27**, 5397 (1992).  
<sup>32</sup>J. Adam and M. D. Rodgers, *Acta Crystallogr.* **12**, 951 (1959); R. E. Hann, P. R. Suttch, and J. L. Pentecost, *J. Am. Ceram. Soc.* **68**, C-285 (1985).  
<sup>33</sup>F. Liu, S. H. Garofalini, D. Kingsmith, and D. Vanderbilt, *Phys. Rev. B* **49**, 12528 (1994).  
<sup>34</sup>N. R. Keskar and J. R. Chelikowsky, *Phys. Rev. B* **46**, 1 (1992).  
<sup>35</sup>L. Levien, C. T. Prewitt, and D. J. Weidner, *Am. Mineral.* **65**, 140 (1983).  
<sup>36</sup>N. Tit and M. W. C. Dharma-Wardana, *J. Appl. Phys.* **86**, 387 (1999).  
<sup>37</sup>R. W. G. Wyckoff, *Crystal Structure*, 4th ed. (Interscience, New York, 1974), and references therein.  
<sup>38</sup>M. Rubinstein and R. Colby, *Polymer Physics* (Oxford University

- Press, New York, 2003).
- <sup>39</sup>C. A. Balans, *Advanced Engineering Electromagnetics* (Arizona State University, New York, 1989).
- <sup>40</sup>J. H. Daly, D. Hayward, and R. A. Pethrick, *J. Phys. D* **19**, 885 (1986).
- <sup>41</sup>L. E. Ramos, J. Furthmuller, and F. Bechstedt, *Phys. Rev. B* **69**, 085102 (2004).
- <sup>42</sup>W. G. Wolf, S. B. Stanley, and K. A. McCarthy, *American Institute of Physics Handbook* (McGraw-Hill, New York, 1963), p. 24.